

# Multiscale Kernels for Enhanced U-shaped Network to Improve 3D Neuron Tracing

Heng Wang<sup>1</sup> Donghao Zhang<sup>1</sup> Yang Song<sup>2</sup> Siqi Liu<sup>3</sup> Heng Huang<sup>4</sup> Mei Chen<sup>5</sup>  
Hanchuan Peng<sup>6</sup> Weidong Cai<sup>1</sup>

<sup>1</sup>School of Computer Science, University of Sydney, Australia

<sup>2</sup>School of Computer Science and Engineering, University of New South Wales, Australia

<sup>3</sup>Digital Services, Digital Technology & Innovation, Siemens Healthineers, USA

<sup>4</sup>Department of Electrical and Computer Engineering, University of Pittsburgh, USA

<sup>5</sup>Department of Informatics, University of Albany State University of New York, USA

<sup>6</sup>Allen Institute for Brain Science, USA

## Abstract

*Digital neuron morphology reconstruction from three-dimensional (3D) volumetric optical microscope images is an important procedure to rebuild the connections and structures of neural circuits. Even though many approaches have been proposed to achieve precise tracing, it is still a challenging task especially when images are polluted by noise or have discontinuity in their neuron structures. In this paper, we propose a new framework to overcome these issues by performing neuron segmentation prior to tracing. Our proposed framework adopts a novel 3D U-shaped convolutional neural network (CNN) with multiscale kernel fusion and spatial fusion to perform the image segmentation. We then perform the iterative back-tracking tracing algorithm on the output of the network. Evaluated on the Janelia dataset from the BigNeuron project, our proposed framework achieves competitive tracing performance.*

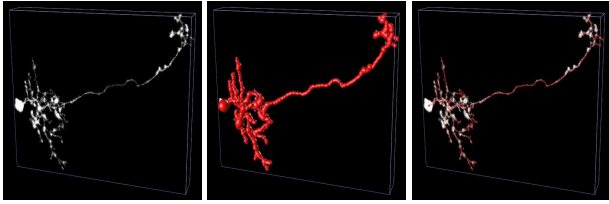
## 1. Introduction

Neuron morphology leads a critical role in the analysis of neural circuits. 3D neuron reconstruction, also known as 3D neuron tracing, is a systematic procedure that rebuilds the tree-shaped model from optical microscopic images. In the field of computational neuroscience, acquiring the reconstructed neuronal structures such as curvilinear arbours and blob-shaped soma [38] is essential to determining a neuron's identity as well as its connectivity and its functionality within the nervous system. Most of the 3D neuron morphology models generated in the past were collected manually or semi-automatically by biologists. Some of these

traditional manual labeling techniques are genetic labeling [20], immunolabeling [22], and bulk dye loading [11]. This is highly time-consuming and labor-intensive for large datasets with varying neuron types. Making the rebuilding procedure automatic and efficient has become one of the major motivations in this field. Hackathon events such as the DIADEM challenge [4] and the BigNeuron challenge [25] were hosted to develop fast and accurate algorithms by offering open-access datasets and complementary software tools.

Over the past few decades, many methods have been proposed to automatically perform 3D reconstruction of neuron morphology. A shape analysis method, Rayburst sampling algorithm [35], was proposed to represent the anisotropic and irregularly shaped structures such as dendritic spine heads with greater accuracy and was adopted by [27] to improve the automatic 3D neuron tracing. MOST [24] then extended it in a marching fashion to better obtain the global tree-like neuronal shape. APP [26], APP2 [36], MOST [24], and Snake [34] are traditional algorithms that start the tracing from the seeds (i.e. the soma) to neuronal branch termini while the recent Rivulet [37, 17], Rivulet2 [19], and the exhaustive tracing algorithm [30] trace from the furthest neuronal points backwards iteratively.

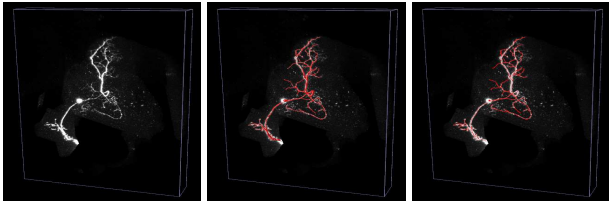
However, most of these automatic algorithms still tend to be error-prone when the images have low quality. Due to the limits of optical microscope imaging, the 3D neuron light microscopic image stacks always contain inevitable background noise and small gaps along neural branches. Affected by the unevenly distributed fluorescent markers, there is often discontinuity within the structures of neurons. The examples for these two challenges are shown in Fig. 1 and Fig. 2 respectively. As indicated by Fig. 1(b)



(a) 3D optical raw image (b) Gold standard (c) Gold standard in line-mode

Figure 1. A highly disconnected fly neuron image and its annotated ground truth. Gold standard is ground truth labelled by a neuroscientist and verified by at least three experts.

and Fig. 2(b), the radius for each neural voxel has been provided in the ground truth annotation files. To make the visualization clearer, we also put gold standard ground truth without radius (line-mode) to emphasize the tree structures. In Fig. 1, the fluorescent markers on the curvilinear neuron fibres are too narrow to be captured by the confocal microscopes, which is likely to result in under-segmentation during tracing. The 3D fly neuron structures in Fig. 2 are immensely contaminated by background noise thus making it difficult to distinguish the neural structures especially the curvilinear arbours.



(a) 3D optical raw image (b) Gold standard (c) Gold standard in line-mode

Figure 2. An overly noisy fly neuron image and its annotated ground truth. Gold standard is ground truth labelled by a neuroscientist and verified by at least three experts.

Existing state-of-the-art neuron extraction methods typically consist of pre-processing the optical image, tracing the neuron branches, and post-processing the traced image [19]. Neuronal structure segmentation from the background voxels is one of the key for pre-processing a neuron image with the aim of eliminating noise and bridging the small gaps along neurite branches. In existing methods, segmentation is normally conducted by applying adaptive or manual thresholding. It is less effective when datasets lack such global threshold annotations. To eliminate the human intervention, we propose a novel 3D convolutional neural network (CNN) model to perform the image segmentation. We examined the performance of our method using the *Janelia* dataset from the BigNeuron project [25]. We also compared our proposed network to a baseline U-Net model [6] by performing the same tracing task. The results

indicate that our proposed framework enhanced the tracing accuracy and also exceeded other threshold-aided state-of-the-art algorithms.

## 2. Related Work

Combining different techniques, automatic 3D neuron morphology reconstruction methods generally involve pre-processing a raw neuron image, defining starting points, tracing the global tree-like neuronal structures, and post-processing the traced image. Traditional algorithms can be divided according to the tracing direction. Rayburst sampling algorithm [35, 27] conducts multidirectional radius sampling to preserve the anisotropic and irregularly shaped 3D structures. It achieves precise shape representation by shooting a ray from inside the 3D model to the surface. Later a continuous radius is estimated to simulate the tubular neuronal branches. MOST [24] further extends this algorithm to follow a marching pattern by tracing from seeds along the curvilinear arbours recursively. Similarly, APP [26], APP2 [36], and Snake [34] also trace from automatically detected seed points. Snake generates an open curve active contour from the 3D image. The mixture of deforming forces computed by the Gradient Vector Flow (GVF) and stretching forces calculated by estimating the fiber orientations is applied as a guidance to the tracing. A set of additional control criteria are also adopted to monitor the tracing in a more precise way. This tracing method additionally applies a series of preprocessing techniques to standardize different image settings from various datasets to make the tracing phase smoother. Unlike performing the tracing all at once, APP and APP2 generate an initial reconstruction to include all the possible neuronal regions and then prune as much as they can to make the reconstructed structures precise. The common trait of these two all-path pruning methods is the way they produce the initial reconstruction. For each possible neuronal points, they trace along the geodesic shortest path from the detected seed points. In APP, the redundant structures are removed adaptively following the maximal-covering minimal-redundant (MCMR) subgraph algorithm. While in APP2, they prune wrongly traced paths using a long-segment-first hierarchical procedure. This new pruning technique turns out to preserve the connectivity while enhancing the tracing accuracy. A new grey-scale weighted distance transform (GWDT) mapping was also proposed in APP2 for improving the initial reconstruction. Recently, Rivulet [37, 17] and Rivulet 2 [19] proposed a new tracing concept as they start the tracing from the geodesic furthest points and iteratively go back to the seed points. This prevents the tracing from stopping early with the presence of small gaps along neurite branches. Neural network techniques are also considered to enhance the performance. SmartTracing [5] is a self-learning-based learning approach. It trains on neuronal re-

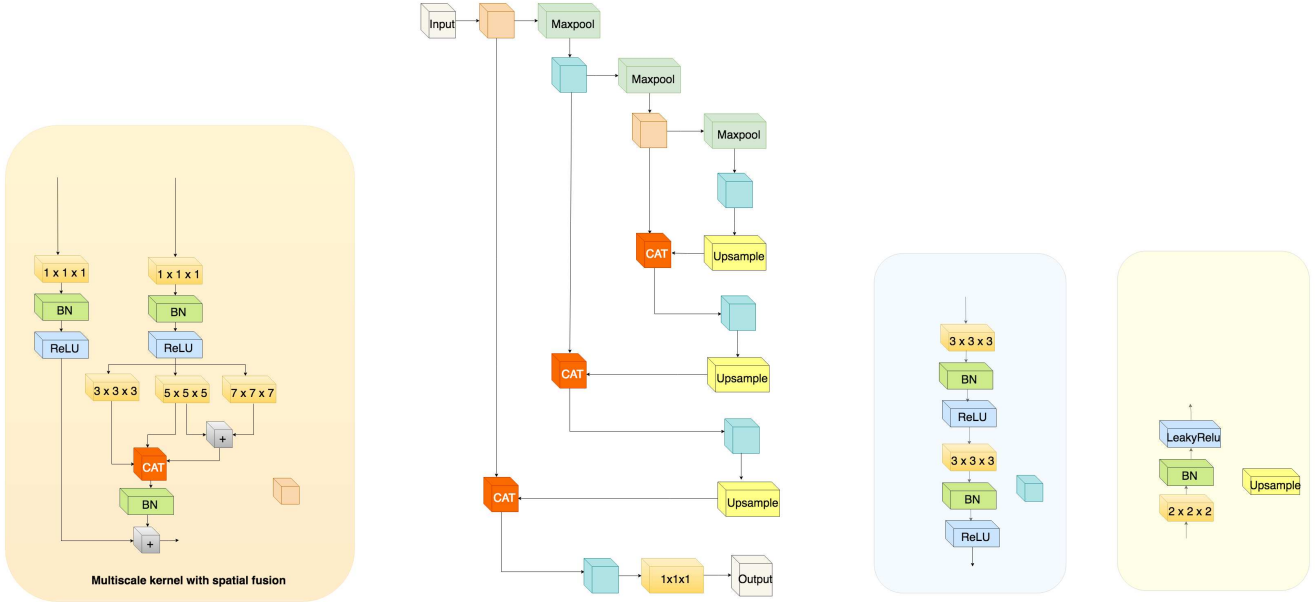


Figure 3. Architecture of our proposed segmentation network.

gions with high possibilities generated by existing neuron tracing algorithms. The trained network is used as a neuronal region detector.

Most of the algorithms stated above focus on improving the intermediate tracing phase. They usually apply an adaptive or manual threshold to generate a basic segmented structures as pre-processing. However, this simple segmentation technique is error-prone especially with the presence of noise and disconnected segments. One way to reduce the dependency on human intervention and make the pre-processing process efficient is to apply deep learning techniques in neuron image segmentation. CNNs like U-Net [6] and V-Net [23] are popular models for medical image segmentation. They use convolutional layers to represent the different scales of features which are too abstract to extract in traditional non-CNN algorithms. More advanced models such as Res3dNet [13] propose a compact and efficient voxel-based neural network combined residual connections and dilated convolutions. The shortcut in the residual blocks allows loss to flow backwards successfully and reserves more details. Convolution with different dilated rate also improves the segmentation results by learning features from different scales of receptive fields. Other variants [10, 8, 16] of CNNs used for semantic segmentation have also been adopted in biomedical image segmentation to improve the general segmentation performance with different purposes such as membrane segmentation [14], brain tumor segmentation [15], and cell segmentation [39]. Recently, an efficient teacher-student network [33] was proposed to enhance the inference performance of neuron segmentation. In addition, the loss used in 3D biomedical image segmentation

tasks to guide the learning is critical, among which there are dice loss [23], generalised dice loss [29], sensitivity-specificity loss [3], and wasserstein dice loss [7].

However, rare attempts have been made to use CNN-based image segmentation techniques for 3D neuron reconstruction. The irregular structures in various neuron types are difficult to generalize. A triple-crossing 2.5D CNN [18] utilizes the information along different dimensions to examine the curvilinear neuronal arbours. An end-to-end image segmentation network [12] was proposed to enhance the performance of tracing algorithms by learning precise feature representations through convolutional blocks.

Unlike previous methods, our proposed method uses a U-shaped multiscale kernel fusion network to aggregate the information learnt from different scales of convolutional filters. A large kernel size in the filter leads to a large receptive field which contains more context information while small kernel size filters focus on local features only. The information fusion among them makes the network robust to various scales of neuron structures thus reducing the effect of noise and discontinuity in the 3D neuron images.

### 3. Methods

#### 3.1. Overview

To enhance the 3D neuron tracing performance, we propose a novel framework which combines a multiscale kernel fusion network for neuron segmentation with an iterative tracing algorithm. Given a raw 3D optical microscope image  $I(x)$ , we put it into the fusion network to generate the segmentation output  $B(x)$ . The segmentation net-

work learns different scales of neuronal structure features from blob-shaped spine head to curvilinear arbour by fusing multiscale convolutional outputs. The details of this architecture are elaborated in Section 3.2 and Section 3.3. The ground truths of segmentation network is generated by the distance-transform of SWC file in Section 3.4. We then perform an iterative backtracking tracing algorithm on this segmented neuron image  $B(x)$  to get the final reconstruction output which are discussed in Section 3.5.

### 3.2. Multiscale Kernel Fusion Network

As shown in Fig. 3, we design a novel 3D image segmentation network, which is a variant of 3D U-Net [6]. Similar to U-Net, we have 7 convolutional blocks (CBs) and 3 deconvolutional blocks (DBs). The difference is that for the first and third CBs, we replace them with a novel spatial fusion convolution block (SFCB). We aggregate the information of different receptive fields by concatenating them together. The details are discussed in Section 3.3. Except for those in the SFCB, the size of the convolutional filters of all CBs is  $3 \times 3 \times 3$ . We use DBs to perform the up-sampling process. It has a deconvolutional kernel of size  $2 \times 2 \times 2$ . The number of convolutional filters from the first to the last CB are 16, 32, 64, 128, 64, and 32 respectively and that of deconvolutional filters from the first to the last DB are 64, 32, and 16 respectively. In CB, each convolutional layer is followed by a 3D batch normalization [9] and a ReLU activation function. Similarly, in DB, we follow the same pattern except that leaky ReLU is applied instead of ReLU. We adopt a 3D cross entropy loss with the weight ratio  $w_0$  defined as the weight of the background label. We penalize more on foreground error since the percentage of foreground voxels is always much less than that of background voxels.

### 3.3. Spatial Fusion Convolution Block

We upgrade the traditional convolutional block to a compact and efficient spatial fusion block with three different receptive fields being deployed. As illustrated by the left diagram in Fig. 3, the size of the convolution kernels inside this block is  $3 \times 3 \times 3$ ,  $5 \times 5 \times 5$ , and  $7 \times 7 \times 7$  respectively. We further aggregate the information among the convolution parallel by fusing the last two feature maps since they contain more context-related information. After fusing all these feature maps together by concatenation, we add a shortcut from the input to the fusion result to preserve more detailed information. The number of channels gets doubled after this block.

### 3.4. Scale Space Distance Transformed Ground Truth

To train the segmentation network, we generate the segmentation ground truth from the SWC file provided with the

training images. The SWC format is a standardized neuro-morphometric format which stores the information of each neuronal point on a neuron image as well as the connectivity among them. It has been widely used for neuronal morphology analysis and neuron reconstruction sharing. Each line in the SWC file records a 7-tuple properties of a neuronal point. Among these properties are the voxel’s identifier number (usually an integer incrementing from 1), type, x coordinate, y coordinate, z coordinate, radius, and the identifier number of its parent. Given a pair of 3D neuron image and its SWC file, we generate a binary map of the same volume with the input image. The intensity of the voxel is 1 if it is recorded by the corresponding SWC file or inside the radius area of any point on the SWC file otherwise it is 0. To highlight the centralines of the neuron structure, we assign higher intensity values to neuronal regions near the centralines by performing a scale space distance transform method on the binary map generated from the SWC file. This synthetic centerline transform map displays the distance between each point with the centralines. The intensity map transformed from the distance map is defined as:

$$i(p, r) = e^{\alpha \cdot (1 - \frac{DT(p,r)}{\beta})} - 1 \quad (1)$$

where  $p$  is the 3D coordinate,  $r$  is the radius, and  $DT(p, r)$  is the distance transform map;  $\alpha$  and  $\beta$  are 6 and 5, respectively. We then normalize  $i(p, r)$  and binarize it as below:

$$GT(p, r) = \begin{cases} 0 & \text{if } i(p, r)_{normalized} \leq 0 \\ 1 & \text{otherwise} \end{cases} \quad (2)$$

### 3.5. Iterative Backtracking Based on Fast Marching

The segmented neuronal structures image generated by the multiscale kernel fusion network in Section 3.2 is then passed through the tracing algorithm to perform the final reconstruction. Following the pattern of MEIT [32], we adaptively trace the neuronal structures. We generate a time-crossing map  $T$  based on the binary map by performing Fast Marching algorithm [28, 2, 31]. It represents the shortest time to traverse from the source points to the current position. We obtain the time-crossing map  $T$  by solving the following Eq. (3):

$$F = \frac{dx}{dT}, \quad |\nabla T|F = 1, \quad T(\Gamma_0) = 0 \quad (3)$$

where  $F$  is the evolution speed and  $\Gamma_0$  is the initial condition [1].

Then,  $T$  is further simplified as:

$$T(x) = \min_{P(s,x)} \int_0^L \left( \frac{F(P(t))}{\max F} \right)^4 dt \quad (4)$$

where  $P(s,x)$  are possible paths  $L$  from the starting point  $s$  to  $x$ .

The next point to be included in the reconstructed neuronal structures is decided by manipulating the subvoxel gradient with Runge-Kutta [17] defined as:

$$\left\{ \begin{array}{l} k_1 = 0.5\alpha/\max(\|\nabla T(p_i)\|, 1) \\ p_{i,1} = p_i - k_1 \\ k_2 = 0.5\alpha/\max(\|\nabla T(p_{i,1})\|, 1) \\ p_{i,2} = p_{i,1} - k_2 \\ k_3 = \alpha/\max(\|\nabla T(p_{i,2})\|, 1) \\ p_{i,3} = p_{i,2} - k_3 \\ k_4 = \alpha/\max(\|\nabla T(p_{i,3})\|, 1) \\ p_{i+1} = p_i - (k_1 + 2k_2 + 2k_3 + k_4)/6 \end{array} \right. \quad (5)$$

where  $k_1, k_2, k_3, k_4$  are the direction vectors at the corresponding point  $p$ , and  $\alpha$  is a constant set to 1 in our experiment. A special case is applied to prevent the tracing from trapping at a local minimal, for which the momentum [19] update rule is defined as:

$$p_{i+1} = 2p_i - p_{i-2} \text{ if } \|p_{i+1} - p_i\|_2^2 \text{ is small} \quad (6)$$

## 4. Experiments and Results

### 4.1. Experiment Setting

We evaluated our proposed framework using the Janelia dataset, which is part of the BigNeuron project. Produced by a combinatorial multicolor stochastic labeling method Brainbow [21], this Janelia dataset holds a variety of neuronal morphologies of adult *Drosophila* nervous system by optical microscopy. It has 42 light microscope images in total. We extracted 38 images for training from which we took 3 images for validation. We used 4 images for testing. The average sizes for training, validation, and testing were  $196 \times 197 \times 176$ ,  $206 \times 219 \times 41$ , and  $262 \times 159 \times 181$ , respectively. For each of these images, we provide a distance transformed ground truth label as discussed in Section 3.4.

During each training epoch, a patch with the size of  $128 \times 128 \times 64$  is randomly extracted from a sequence of 8 images as the input for training the image segmentation network. The weight ratio  $w_0$  is fixed as 0.45. We applied data augmentation techniques such as random flipping and random-angle rotation along different axes to enlarge the dataset. This network was trained using the Adam optimizer with a learning rate of  $1 \times 10^{-3}$  and a weight decay of  $5 \times 10^{-4}$ . To generate the final prediction from a whole 3D image stacks, we placed a sliding window on the input testing image adaptively and then combine the patch-level outputs together.

### 4.2. Results and Analysis

Our proposed segmentation network was compared to the baseline 3D U-Net by investigating the similarities be-

Table 1. The quantitative segmentation comparison between 3D U-Net and our proposed network.

Fly Testing (4)	Precision	Recall	F1	Precision	Recall	F1
Fly1	0.56	0.79	<b>0.66</b>	0.58	0.74	0.65
Fly2	0.37	0.84	<b>0.52</b>	0.32	0.90	0.47
Fly3	0.25	0.54	<b>0.35</b>	0.26	0.51	0.34
Fly4	0.35	0.33	<b>0.34</b>	0.35	0.25	0.29
average	0.38	0.63	<b>0.47</b>	0.38	0.60	0.44
std	0.13	0.24	<b>0.15</b>	0.14	0.28	0.16
method	<b>Proposed</b>			UNet3D		

Table 2. The quantitative comparison of reconstructed points with SWC ground truth between our proposed method, Ensemble, TreMap [40], APP2, Snake, Neutube, MOST, and SmartTracing. The number beside the dataset name is the number of 3D images in each dataset. The number of the successful reconstructions are shown beside the method name.

Fly	Precision	Recall	F1
<b>Proposed (4/4)</b>	$0.79 \pm 0.24$	$0.95 \pm 0.05$	<b><math>0.85 \pm 0.16</math></b>
Ensemble (4/4)	$0.1 \pm 0.04$	<b><math>0.99 \pm 0.03</math></b>	$0.684 \pm 0.07$
TreMap (4/4)	$0.80 \pm 0.16$	$0.38 \pm 0.19$	$0.48 \pm 0.14$
APP2 (4/4)	$0.87 \pm 0.09$	$0.33 \pm 0.28$	$0.42 \pm 0.31$
Snake (4/4)	<b><math>0.9 \pm 0.05</math></b>	$0.57 \pm 0.22$	$0.68 \pm 0.17$
Neutube (4/4)	$0.88 \pm 0.10$	$0.52 \pm 0.18$	$0.63 \pm 0.15$
MOST (4/4)	$0.33 \pm 0.28$	$0.26 \pm 0.21$	$0.2 \pm 0.13$
SmartTracing (3/4)	$0.75 \pm 0.06$	$0.97 \pm 0.02$	$0.84 \pm 0.05$

tween them and the distance transformed ground truth label in Section 3.4. The major difference between our proposed segmentation network and the 3D U-Net network is the multiscale kernels. We trained and tested our baseline using exactly the same training, validation, and testing set. We display the results using precision, recall, and F1-score in Table 1. The precision, recall, and F1-score are defined as:

$$\begin{aligned} Precision &= \frac{TP}{TP + FP} \\ Recall &= \frac{TP}{TP + FN} \\ F1 &= \frac{2 \times Precision \times Recall}{Precision + Recall} \end{aligned} \quad (7)$$

where TP, FP, and FN represent the true positive, false positive and false negative voxels that were segmented by the compared networks. Tested on 4 images, our proposed network outperforms the baseline 3D U-Net. After using spatial fusion, the proposed network reserves more features thus improving the recall in most cases. It is also noticeable that our proposed network is more stable than U-Net.

In addition, we compared our proposed overall framework with 7 other state-of-the-art tracing algorithms on precision, recall, and F1-score, as shown in Table 2. The precision, recall, and F1-score are defined similarly in Equation 7. However, here the TP, FP, and FN are collected as the nodes from the generated SWC by different algo-

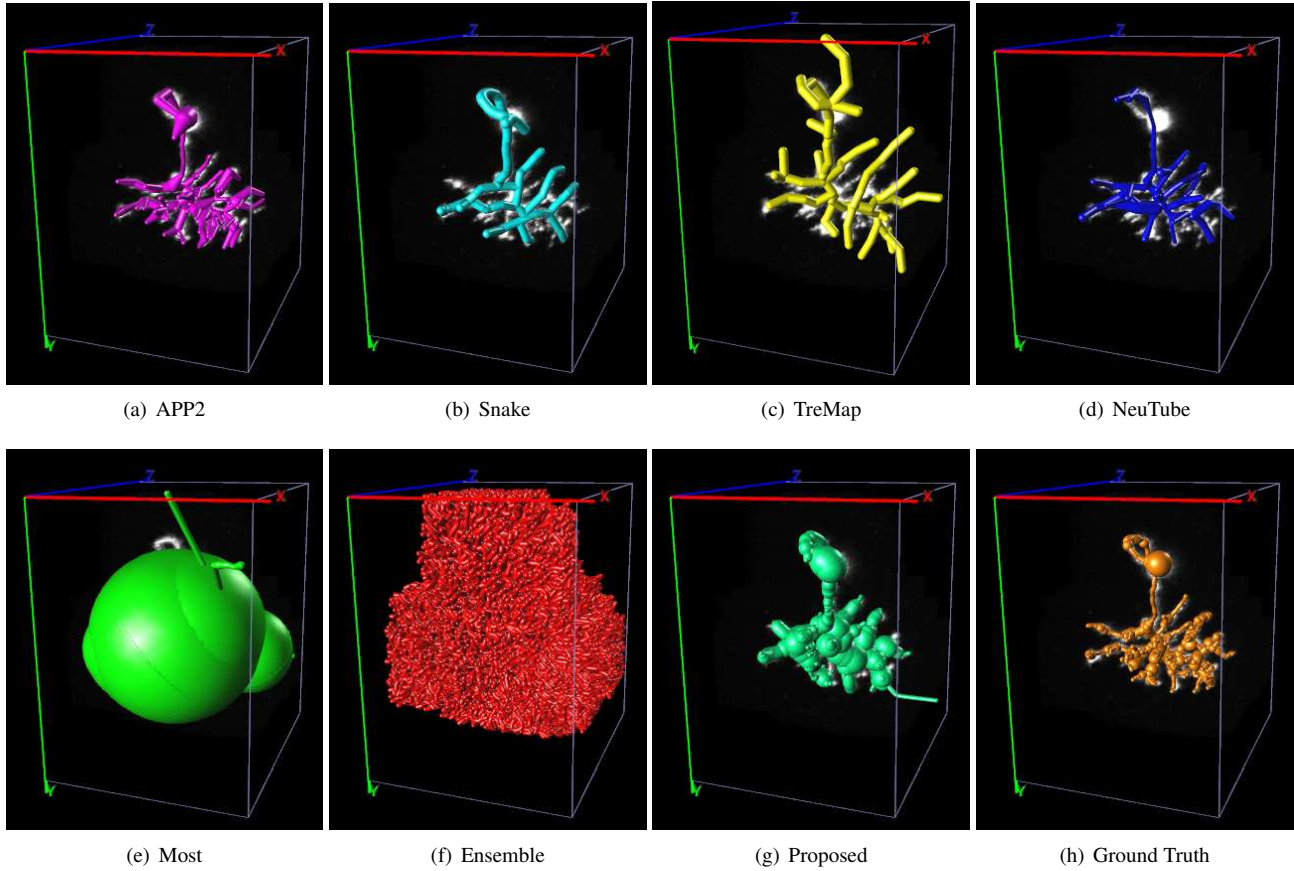


Figure 4. Visualization of different tracing algorithms for a Fly1 image.

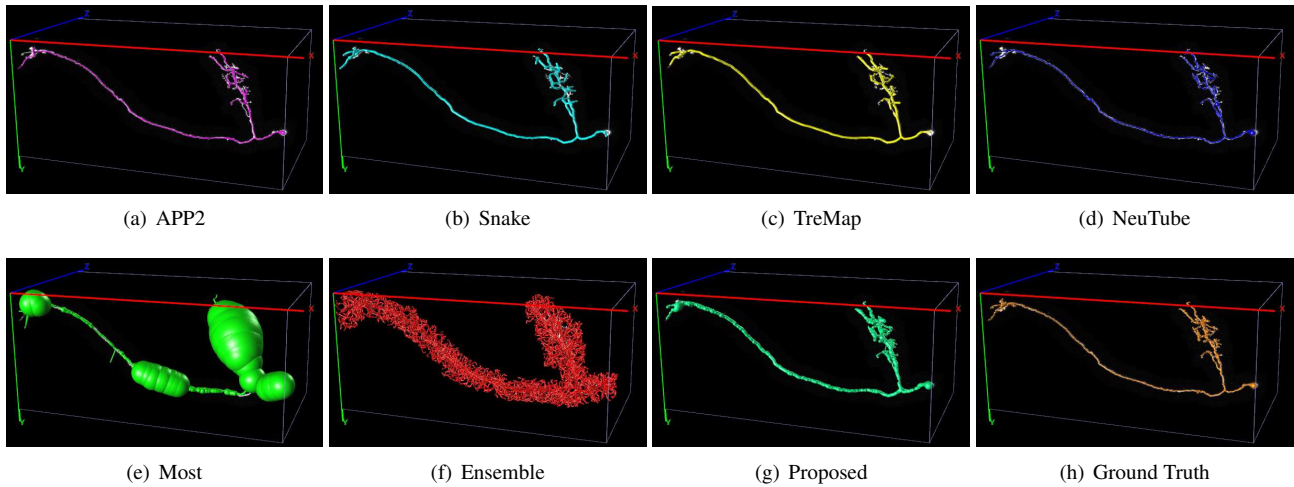


Figure 5. Visualization of different tracing algorithms for a Fly2 image.

rithms instead of voxels from binary segmentations. While SmartTracing failed to trace all of the images, our proposed framework successfully reconstructed all the testing images and achieve the best accuracy among all these algorithms. Since some algorithms such as APP2, TreMap, and MOST

depend on the choice of a strict threshold, they cannot guarantee that neuronal structures would not be removed by accident. This leads to reduction in the number of correctly traced points. However, our proposed method produce the binary result without any threshold needed which results in

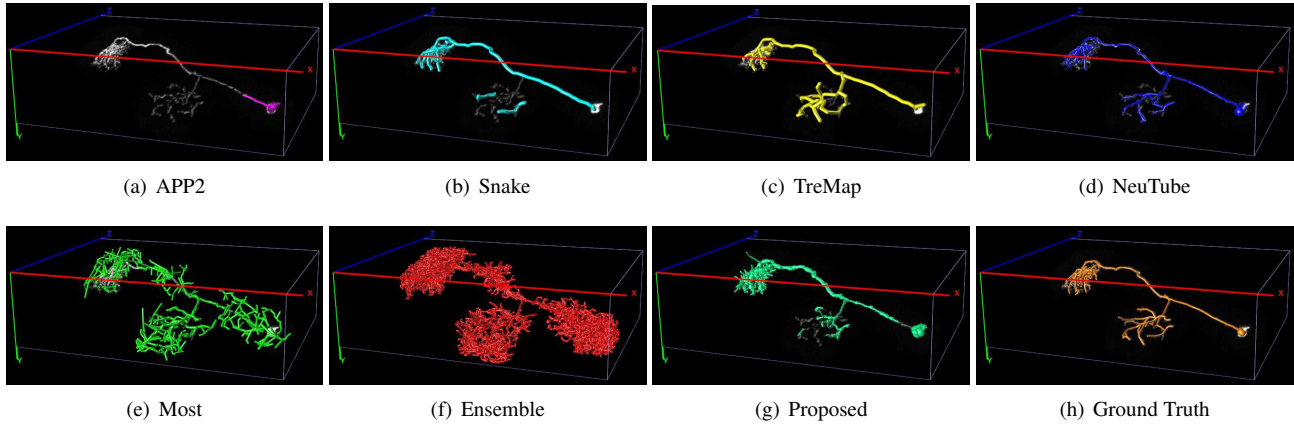


Figure 6. Visualization of different tracing algorithms for a Fly3 image.

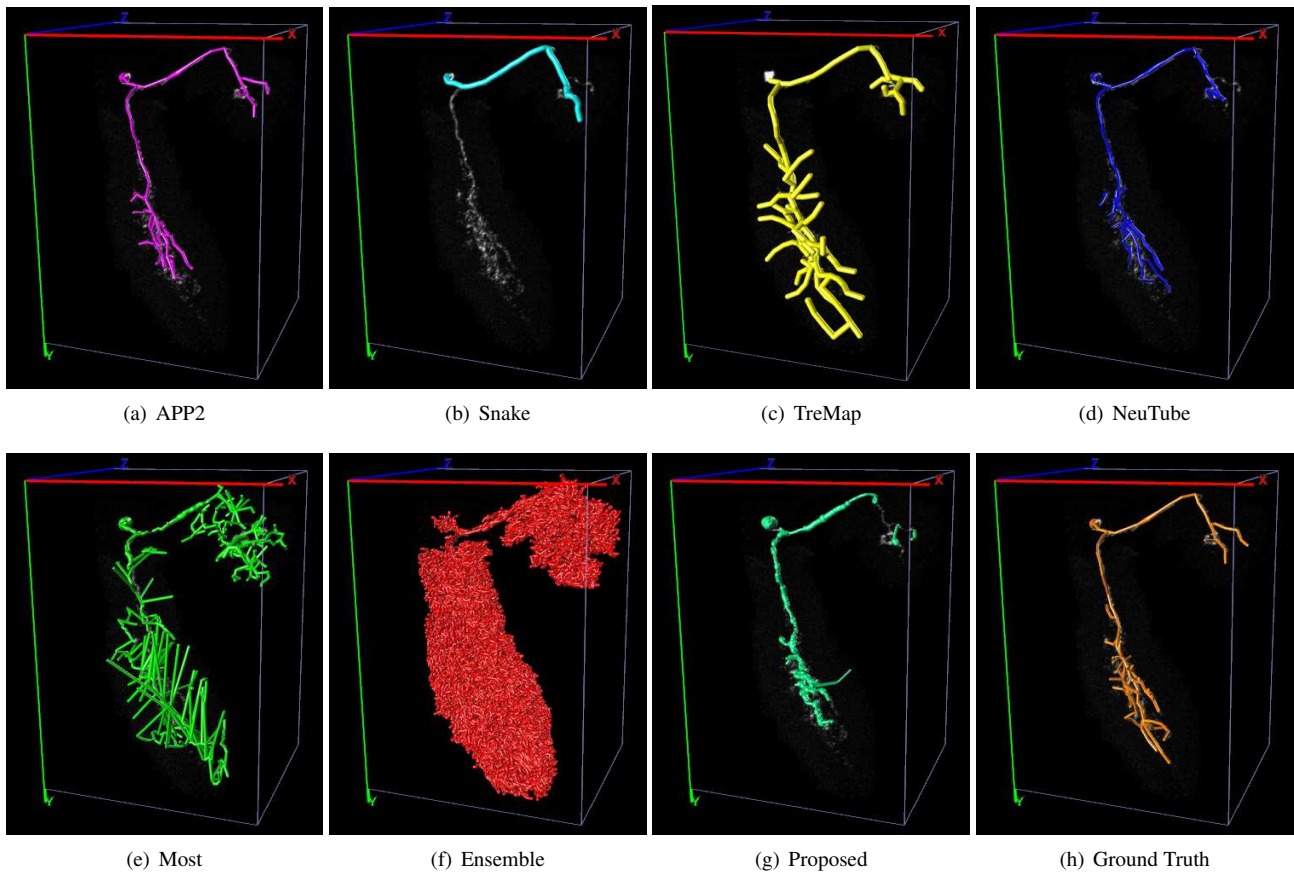


Figure 7. Visualization of different tracing algorithms for a Fly4 image.

better recall.

We present the visualization of tracing results using 7 different tracing algorithms. As shown in Fig. 4, while most methods fail to reconstruct the soma (usually the one with the largest radius) with the presence of noises, our proposed method achieves the most similar reconstruction compared to the ground truth. In Fig. 5, our proposed method achieved

the state-of-the-art result by reconstructing exactly like the ground truth. Fig. 6 and Fig. 7 show competitive tracing results. If more data is given, the generalization ability of the proposed network can be improved and the results could be better and more stable.

## 5. Conclusion

We propose a novel framework to perform neuron reconstruction from 3D optical microscopic images. To eliminate irrelevant structures such as noise and bridge the small gaps along neurite branches, we design a 3D multiscale kernel fusion network to segment the neuronal structure as a pre-processing step. We then take the segmented image into the iterative backtracking algorithm to generate the final reconstruction. Our evaluation on the Janelia dataset shows that our proposed method could improve the performance of neuron tracing algorithms and outperform other state-of-the-art neuron reconstruction algorithms.

## References

- [1] D. Adalsteinsson and J. A. Sethian. A fast level set method for propagating interfaces. *Journal of Computational Physics*, 118(2):269–277, 1995.
- [2] S. Basu and D. Racoceanu. Reconstructing neuronal morphology from microscopy stacks using fast marching. In *ICIP*, pages 3597–3601. IEEE, 2014.
- [3] T. Brosch, Y. Yoo, L. Y. Tang, D. K. Li, A. Traboulsee, and R. Tam. Deep convolutional encoder networks for multiple sclerosis lesion segmentation. In *MICCAI*, pages 3–11. Springer, 2015.
- [4] K. M. Brown, G. Barrionuevo, A. J. Canty, V. De Paola, J. A. Hirsch, G. S. Jefferis, J. Lu, M. Snippe, I. Sugihara, and G. A. Ascoli. The diadem data sets: representative light microscopy images of neuronal morphology to advance automation of digital reconstructions. *Neuroinformatics*, 9(2-3):143–157, 2011.
- [5] H. Chen, H. Xiao, T. Liu, and H. Peng. Smarttracing: self-learning-based neuron reconstruction. *Brain Informatics*, 2(3):135–144, 2015.
- [6] Ö. Çiçek, A. Abdulkadir, S. S. Lienkamp, T. Brox, and O. Ronneberger. 3D U-Net: learning dense volumetric segmentation from sparse annotation. In *MICCAI*, pages 424–432. Springer, 2016.
- [7] L. Fidon, W. Li, L. C. Garcia-Peraza-Herrera, J. Ekanayake, N. Kitchen, S. Ourselin, and T. Vercauteren. Generalised wasserstein dice score for imbalanced multi-class segmentation using holistic convolutional networks. In *MICCAI workshop*, pages 64–76. Springer, 2017.
- [8] L. Fidon, W. Li, L. C. Garcia-Peraza-Herrera, J. Ekanayake, N. Kitchen, S. Ourselin, and T. Vercauteren. Scalable multimodal convolutional networks for brain tumour segmentation. In *MICCAI*, pages 285–293. Springer, 2017.
- [9] S. Ioffe and C. Szegedy. Batch normalization: Accelerating deep network training by reducing internal covariate shift. *arXiv preprint arXiv:1502.03167*, 2015.
- [10] K. Kamnitsas, C. Ledig, V. F. Newcombe, J. P. Simpson, A. D. Kane, D. K. Menon, D. Rueckert, and B. Glocker. Efficient multi-scale 3D cnn with fully connected crf for accurate brain lesion segmentation. *Medical Image Analysis*, 36:61–78, 2017.
- [11] J. L. Lanciego and F. G. Wouterlood. A half century of experimental neuroanatomical tracing. *Journal of Chemical Neuroanatomy*, 42(3):157–183, 2011.
- [12] R. Li, T. Zeng, H. Peng, and S. Ji. Deep learning segmentation of optical microscopy images improves 3D neuron reconstruction. *IEEE Transactions on Medical Imaging*, 36(7):1533–1541, 2017.
- [13] W. Li, G. Wang, L. Fidon, S. Ourselin, M. J. Cardoso, and T. Vercauteren. On the compactness, efficiency, and representation of 3D convolutional networks: brain parcellation as a pretext task. In *IPMI*, pages 348–360. Springer, 2017.
- [14] D. Liu, D. Zhang, S. Liu, Y. Song, H. Jia, D. Feng, Y. Xia, and W. Cai. Densely connected large kernel convolutional network for semantic membrane segmentation in microscopy images. In *ICIP*, pages 2461–2465. IEEE, 2018.
- [15] D. Liu, D. Zhang, Y. Song, F. Zhang, L. J. O'Donnell, and W. Cai. 3D large kernel anisotropic network for brain tumor segmentation. In *ICONIP*, pages 444–454. Springer, 2018.
- [16] S. Liu, D. Xu, S. K. Zhou, O. Pauly, S. Grbic, T. Mertelmeier, J. Wicklein, A. Jerebko, W. Cai, and D. Comaniciu. 3D anisotropic hybrid network: Transferring convolutional features from 2D images to 3D anisotropic volumes. In *MICCAI*, pages 851–858. Springer, 2018.
- [17] S. Liu, D. Zhang, S. Liu, D. Feng, H. Peng, and W. Cai. Rivulet: 3D neuron morphology tracing with iterative backtracking. *Neuroinformatics*, 14(4):387–401, 2016.
- [18] S. Liu, D. Zhang, Y. Song, H. Peng, and W. Cai. Triple-crossing 2.5D convolutional neural network for detecting neuronal arbours in 3D microscopic images. In *MICCAI Workshop*, pages 185–193. Springer, 2017.
- [19] S. Liu, D. Zhang, Y. Song, H. Peng, and W. Cai. Automated 3D neuron tracing with precise branch erasing and confidence controlled back tracking. *IEEE Transactions on Medical Imaging*, 37(11):2441–2452, 2018.
- [20] J. Livet, T. Weissman, H. Kang, R. Draft, J. Lu, R. Bennis, J. Sanes, and J. Lichtman. Transgenic strategies for combinatorial expression of fluorescent proteins in the nervous system. *Nature*, 450(7166):56, 2007.
- [21] J. Livet, T. A. Weissman, H. Kang, R. W. Draft, J. Lu, R. A. Bennis, J. R. Sanes, and J. W. Lichtman. Transgenic strategies for combinatorial expression of fluorescent proteins in the nervous system. *Nature*, 450(7166):56, 2007.
- [22] K. D. Micheva and S. J. Smith. Array tomography: a new tool for imaging the molecular architecture and ultrastructure of neural circuits. *Neuron*, 55(1):25–36, 2007.
- [23] F. Milletari, N. Navab, and S.-A. Ahmadi. V-net: Fully convolutional neural networks for volumetric medical image segmentation. In *3DV*, pages 565–571. IEEE, 2016.
- [24] X. Ming, A. Li, J. Wu, C. Yan, W. Ding, H. Gong, S. Zeng, and Q. Liu. Rapid reconstruction of 3D neuronal morphology from light microscopy images with augmented rayburst sampling. *PLoS one*, 8(12):e84557, 2013.
- [25] H. Peng, M. Hawrylycz, J. Roskams, S. Hill, N. Spruston, E. Meijering, and G. A. Ascoli. Bigneuron: large-scale 3D neuron reconstruction from optical microscopy images. *Neuron*, 87(2):252–256, 2015.

- [26] H. Peng, F. Long, and G. Myers. Automatic 3D neuron tracing using all-path pruning. *Bioinformatics*, 27(13):i239–i247, 2011.
- [27] A. Rodriguez, D. B. Ehlenberger, P. R. Hof, and S. L. Wearne. Rayburst sampling, an algorithm for automated three-dimensional shape analysis from laser scanning microscopy images. *Nature Protocols*, 1(4):2152–2161, 2006.
- [28] J. A. Sethian. *Level set methods and fast marching methods: evolving interfaces in computational geometry, fluid mechanics, computer vision, and materials science*, volume 3. Cambridge university press, 1999.
- [29] C. H. Sudre, W. Li, T. Vercauteren, S. Ourselin, and M. J. Cardoso. Generalised dice overlap as a deep learning loss function for highly unbalanced segmentations. In *DLMIA*, pages 240–248. Springer, 2017.
- [30] Z. Tang, D. Zhang, S. Liu, Y. Song, H. Peng, and W. Cai. Automatic 3D single neuron reconstruction with exhaustive tracing. In *Proc. of ICCV*, pages 126–133, 2017.
- [31] R. Van Uitert and I. Bitter. Subvoxel precise skeletons of volumetric data based on fast marching methods. *Medical Physics*, 34(2):627–638, 2007.
- [32] H. Wang, D. Zhang, Y. Song, S. Liu, R. Gao, H. Peng, and W. Cai. Memory and time efficient 3D neuron morphology tracing in large-scale images. In *DICTA*. IEEE, 2018.
- [33] H. Wang, D. Zhang, Y. Song, S. Liu, Y. Wang, D. Feng, H. Peng, and W. Cai. Segmenting neuronal structure in 3D optical microscope images via knowledge distillation with teacher-student network. In *ISBI*, 2019.
- [34] Y. Wang, A. Narayanaswamy, C. Tsai, and B. Roysam. A broadly applicable 3-D neuron tracing method based on open-curve snake. *Neuroinformatics*, 9(2-3):193–217, 2011.
- [35] S. Wearne, A. Rodriguez, D. Ehlenberger, A. Rocher, S. Henderson, and P. Hof. New techniques for imaging, digitization and analysis of three-dimensional neural morphology on multiple scales. *Neuroscience*, 136(3):661–680, 2005.
- [36] H. Xiao and H. Peng. App2: automatic tracing of 3D neuron morphology based on hierarchical pruning of a gray-weighted image distance-tree. *Bioinformatics*, 29(11):1448–1454, 2013.
- [37] D. Zhang, S. Liu, S. Liu, D. Feng, H. Peng, and W. Cai. Reconstruction of 3D neuron morphology using rivulet backtracking. In *ISBI*, pages 598–601, 2016.
- [38] D. Zhang, S. Liu, Y. Song, D. Feng, H. Peng, and W. Cai. Automated 3D soma segmentation with morphological surface evolution for neuron reconstruction. *Neuroinformatics*, pages 1–14, 2018.
- [39] D. Zhang, Y. Song, D. Liu, H. Jia, S. Liu, Y. Xia, H. Huang, and W. Cai. Panoptic segmentation with an end-to-end cell r-cnn for pathology image analysis. In *MICCAI*, pages 237–244. Springer, 2018.
- [40] Z. Zhou, X. Liu, B. Long, and H. Peng. Tremap: Automatic 3D neuron reconstruction based on tracing, reverse mapping and assembling of 2D projections. *Neuroinformatics*, 14(1):41–50, 2016.